

Adsorption of Xe and Ar on Quasicrystalline Al-Ni-Co

Raluca A. Trasca, Nicola Ferralis, Renee D. Diehl and Milton W. Cole

*Department of Physics and Materials Research Institute,
Pennsylvania State University, University Park, PA 16802*

Abstract

An interaction potential energy between an adsorbate (Xe and Ar) and the 10-fold Al-Ni-Co quasicrystal is computed by summing over all adsorbate-substrate interatomic interactions. The quasicrystal atoms' coordinates are obtained from LEED experiments and the Lennard-Jones parameters of Xe-Al, Xe-Ni and Xe-Co are found using semiempirical combining rules. The resulting potential energy function of position is highly corrugated.

Monolayer adsorption of Xe and Ar on the quasicrystal surface is investigated in two cases: 1) in the limit of low coverage (Henry's law regime), and 2) at somewhat larger coverage, when interactions between adatoms are considered through the second virial coefficient, C_{AAS} . A comparison with adsorption on a flat surface indicates that the corrugation enhances the effect of the Xe-Xe (Ar-Ar) interactions. The theoretical results for the low coverage adsorption regime are compared to experimental (LEED isobar) data.

I. INTRODUCTION

The growth and equilibrium structure of an adsorbed film are dependent on the competing adsorbate-adsorbate and adsorbate-substrate interactions. The laterally aperiodic adsorption potential of a quasicrystalline (QC) surface provides an interesting case of competing interactions for rare gas adsorbates, which favor close-packed monolayer structures in the absence of substrate corrugation. Such incongruity often produces new phenomena which are interesting and exotic on a fundamental level. In this case, because quasicrystals can have radically different physical properties than their periodic counterparts, it also provides a significant tool for the design and growth of thin films having specific properties.

The 10-fold surface of decagonal Al-Ni-Co is aperiodic in the surface plane but periodic in the perpendicular direction [1, 2, 3, 4, 5, 6, 7, 8, 9, 10, 11]. Each quasicrystalline layer comprises an aperiodic array of Al, Ni and Co with points of 5-fold rotational symmetry. Each plane is related to its neighboring planes by a rotation of 36 degrees, producing an ABAB stacking sequence. The structure of this surface has been studied using various techniques, including low-energy electron diffraction (LEED) and scanning tunneling microscopy (STM). A combination of these techniques was used recently to demonstrate that the surface structure of Al-Ni-Co is similar to the bulk structure determined by x-ray diffraction [1], but with a significant relaxation of the top layer and some intralayer buckling [12].

There have been many theoretical studies of physical adsorption on flat substrates and on periodic substrates [13, 14], but none on aperiodic substrates. Recently a rigid-lattice total energy calculation for Al adsorption on a quasiperiodic substrate produced some interesting results concerning the growth and size of Al clusters on the surface [15]. That calculation was carried out by assuming a Lennard-Jones (LJ) potential between the adsorbate Al atoms and the substrate atoms, assuming a bulk-like structure for the surface. Comparisons were made to the results of LEED experiments for the structure, orientation and domain size of the Al film. In particular, the domain size distribution was shown to be a direct consequence of the competing interactions in the substrate and the film.

Because the interactions are weaker, simpler and better known for physisorbed gases, we believe we can gain a fuller understanding of the effects of aperiodicity and symmetry by studying rare gas adsorption on Al-Ni-Co. In this study, we have chosen Xe and Ar as the adsorbates. We have calculated the gas-surface adsorption potential and the adsorption

properties in the low-coverage limit using a virial expansion. The results of these calculations are compared to the results for adsorption on periodic substrates, and to thermodynamic LEED measurements of Xe adsorption on quasicrystalline Al-Ni-Co.

II. EXPERIMENTAL CHARACTERIZATION OF THE AL-NI-CO SUBSTRATE AND XE ADSORPTION

The decagonal Al-Ni-Co quasicrystal has a basic structure that consists of a stack of identical or nearly-identical 5-fold symmetric planes, each related to adjacent ones by a $\pi/5$ rotation [2]. This produces a stacking structure (ABAB) of A and B terminations, with a 10-fold screw axis. A schematic representation of the atomic positions of one of such planes is shown in Figure 1, where the different chemical identities and different local geometry among the same chemical identity are specified. The 10-fold surface presents a contraction (10%) of the first layer and an expansion (5%) of the second layer, with a small degree of intralayer rumpling; in plane reconstruction is minimal, if present. The two-dimensional atomic density of a layer is 0.123 \AA^{-2} [17].

The quasicrystalline d- $Al_{73}Ni_{10}Co_{17}$ (Co-rich phase) sample was grown at Ames National laboratories using the decantation method [19]. The surface was obtained by a cut perpendicular to the 10-fold axis, and then polished as described elsewhere [17] to obtain a surface that was within 0.5° of the ten-fold orientation. The sample preparation in ultra-high vacuum consisted of several cycles of Ar ion bombardment (500 eV ions) for about 45 minutes, followed by annealing for six to eight hours at temperatures up to 1060 K, as measured by a K-type thermocouple in contact with the sample, and an optical pyrometer. The LEED pattern after preparation was observed to have well-defined spots and relatively low intensity between the primary spots, as shown in Figure 2. The impurity level was below detectability, as measured by Auger electron spectroscopy. The symmetry of the LEED pattern is 10-fold, due to the presence of two equivalent surface terminations rotated by 36° [18]. This method of preparation has been shown to produce a surface having a structure that is essentially identical to the bulk structure with the exception of a small degree of surface relaxation [12]. The LEED intensities of the diffraction spots were measured using a rear-view LEED system, with the electron beam at normal incidence to the surface. The LEED adsorption isobars were obtained by holding the Xe pressure at a fixed value while changing

the temperature and acquiring LEED frames. For each frame the integrated spot intensity of a substrate diffraction peak was extracted and plotted versus the acquisition temperature, giving the adsorption isobar [17]. The temperature was measured using a chromel-alumel thermocouple in contact with the sample, in a range between 60 and 140K. The coverage is assumed to be linearly related to the attenuation of the intensity of non-specular substrate diffraction peak in the submonolayer range, where one monolayer is defined by the break in the isobar. Thus, the substrate peak intensity before adsorption is defined to correspond to zero coverage, the intensity at the break in the isobar is defined to be one monolayer, and the intermediate coverages vary inversely and linearly with the intensity [19].

III. CALCULATION OF THE QC INTERACTION POTENTIAL

The calculation of the interaction energy between Xe (or Ar) and the Al-Ni-Co quasicrystalline structure is performed by summing over the LJ pair interactions, Xe-Al, Xe-Ni and Xe-Co. In the following, we will refer to Xe as the adsorbent, but a similar technique is used for Ar for which we will also present results. Lusher and coworkers employed a similar LJ superposition while exploring the growth of Al on Al-Co-Ni QC surface [15]. They assumed that the interaction of Al with each species of the QC is the same. Using this approximation, they were able to predict nanocrystal growth of Al on the QC substrate. Here, we assume that there are two distinct pair interactions: Xe-Al and Xe-TM, where TM stands for either transition metal, Co or Ni.

In order to find the Xe-Al and Xe-TM LJ parameters, we consider adsorption of Xe on separate elemental surfaces of Al(110) and Ni(100). The semiempirical arithmetic combining rules between a Xe gas ($\sigma_{Xe} = 4.1 \text{ \AA}$) and Al or Ni crystals ($\sigma_{Al} = 2.5 \text{ \AA}$, $\sigma_{Ni} = 2.2 \text{ \AA}$) yield $\sigma_{Xe-Al} = 3.3 \text{ \AA}$ and $\sigma_{Xe-TM} = 3.1 \text{ \AA}$. In order to estimate the gas-solid well-depth ϵ parameters, we use the experimental heats of adsorption of Xe on Al(110) ($Q_{Xe-Al} = 190 \text{ meV}$) and on Ni(100) ($Q_{Xe-Ni} = 226 \text{ meV}$) [14], which are basically a measure of the interaction well depth, and the summed pairwise interaction of Xe with Al(110) and Ni(100) crystals, respectively [20]. Finally, we find $\epsilon_{Xe-Al} \simeq 24 \text{ meV}$ and $\epsilon_{Xe-TM} \simeq 23 \text{ meV}$. Notice that the LJ parameters of Xe-Al and Xe-TM are not very different. However, the small difference in the parameter values and the small rumpling of the QC surface play a role in the adsorption potential, as we will show in the following.

Once the Xe-Al and Xe-TM interactions are obtained, we sum them to produce the net Xe-QC interaction. Before discussing the results, we note that they should be interpreted with caution since summation of pair potentials omits effects of electron delocalization, which have been found to occur on metallic substrates [21].

As described in the introduction, the coordinates of the Al-Ni-Co QC atoms were found using LEED data [12]. Due to the QC's aperiodicity, periodic boundary conditions are not appropriate and all substrate atoms have to be considered in calculations. We simplify by selecting a computational cell that is large enough ($56 \text{ \AA} \times 56 \text{ \AA}$) to describe the potential adequately. One way to depict the potential energy $V(\mathbf{r})$ is to construct a “minimum energy surface”, defined as follows: for any surface-parallel position $\mathbf{R}=(x,y)$ we evaluate the position $z(\mathbf{R})=z_{min}(\mathbf{R})$ at which $V(\mathbf{r})$ is a minimum. The resulting well-depth and force constant are called $D(\mathbf{R})$ and $k(\mathbf{R})$, respectively.

A contour plot of the minimum energy surface is shown in Figure 3(a), where the various curves represent isopotential surfaces. The minimum energy surface exhibits the five-fold symmetry of the QC top layer. The big (red) circles correspond to the repulsive regions of the minimum energy surface and are placed on top of the Al-2 species (see Fig. 1). In general, the repulsive part of the minimum energy surface follows closely the distribution of atoms of the top layer, with one exception: the TM atoms which are buried deepest in the first layer. The insensitivity of the interaction energy to those atoms is due to the fact that σ_{Xe-TM} and ϵ_{Xe-TM} are smaller than σ_{Xe-Al} and ϵ_{Xe-Al} .

The most striking feature of the minimum energy surface is its high “corrugation”: local potential minima range from -150 meV to -270 meV. A corrugation of this order was also found on open crystalline structures such as reconstructed Si and Ge [25, 26], but is not usual for metallic surfaces. However, this corrugation does not have the meaning of the hopping barrier between adjacent sites. To better illustrate this point, we plot the lateral variation of $V_{min}(x,y)$ along different path in Figure 3 (b). The full and dashed curves correspond to vertical paths in Fig. 3(a) at $x=-1.6 \text{ \AA}$ and $x=1.6 \text{ \AA}$. The energy difference between local minima and bridges is very irregular and ranges in general from few meV to ≈ 100 meV. We attribute this large range of local minima to the QC's aperiodicity as well as the “holes” (4 \AA width) of its lateral structure [12]. A more complete analysis of the hopping barriers between adjacent sites, with applications in diffusion, involves an identification of the adsorption sites and the saddle points between those. This investigation is in progress.

In order to illustrate the most attractive adsorption sites, in Figure 4 we plot the regions where the adsorption potential has values between -270 meV and -220 meV. McGrath et al argued that quasicrystals could be potentially used as templates for quasicrystalline 2D structures [22, 23]. With this in mind, they have studied adsorption of C_{60} on the Al-Pd-Mn quasicrystal surface, which is known to exhibit depressions of about 7 Å width in a pentagrid structure. STM images at low coverage showed that C_{60} molecules occupy some of those pentagonal holes. In a similar way, Al-Ni-Co is a good candidate as a template for Xe or Ar. It is not clear from Figure 4 if adsorption of Xe at low coverage would lead to a quasicrystalline 2D long-range order structure. Monte Carlo simulations are in progress to investigate this. The interaction energy between Ar and QC shows very similar properties, the main difference being that the local potential minima range from -60 meV to -130 meV.

Another way to depict this highly corrugated potential is provided in Figure 5(a). There is shown the lateral variation of $V(\mathbf{r})$ in the x-z plane for constant z and y=0 (see Figure 3 a). As expected, far from the surface ($z=5.8$ Å), the potential is high and nearly independent of x. Close to the surface ($z=2.8$ Å), the potential exhibits a large and irregular corrugation. An unexpected feature is the following: at some particular values of x ($x \approx -25, -15, -10, -2.5, 5, 20$ Å) the potential is “more” attractive close to the surface ($z = 2.8$ Å), but is “less” attractive at distances farther away from the surface ($z = 3.8, 4.4$ Å). Recently, it has been argued that the corrugation can change sign even for an elemental crystal [24]. This may lead to a possible steering effect on adsorption on the QC, especially important in the process of film growing.

To better understand the interaction potential landscape, we define a “volume density of states” $f(V)$ as follows: $f(V)dV$ equals the volume above the QC surface such that the potential energy lies in the interval $[V, V+dV]$. Then

$$f(V) = \int d\mathbf{r} \delta[V - V(\mathbf{r})] = \int d\mathbf{R} \left\{ \frac{1}{|\partial V/\partial z|^{(1)}} + \frac{1}{|\partial V/\partial z|^{(2)}} \right\} \theta[V + D(\mathbf{R})] \quad (1)$$

where $\theta(x)$ is the unit step function. In the second expression, the denominators equal the magnitudes of the surface-normal forces $|\partial V/\partial z|^{(1)}$ and $|\partial V/\partial z|^{(2)}$ evaluated at the two points (1,2) where $V = V(\mathbf{r})$. Equation 1 has been numerically integrated and the result appears as the full curve in Figure 5(b). Note that the full curve exhibits a broad maximum around -150 meV, due to the heterogeneity of the substrate. We may understand this by considering the behavior of $f(V)$ in two limits, low V and high V. The region of the

potential energy minimum (low V) is particularly important. At a given (\mathbf{R}) , this may be evaluated with a local harmonic approximation : $V(\mathbf{r}) \simeq -D(\mathbf{R}) + k(\mathbf{R})[z - z_{min}(\mathbf{R})]^2/2$ and $|\partial V/\partial z|^{(1)} \simeq |\partial V/\partial z|^{(2)} = [2k(\mathbf{R})(V + D(\mathbf{R}))]^{1/2}$. Therefore, $f(V)$ becomes:

$$f_{har}(V) = \int d\mathbf{R} \theta[V + D(\mathbf{R})] \sqrt{\frac{2}{k(\mathbf{R})(V + D(\mathbf{R}))}} \quad (2)$$

The local harmonic approximation for the heterogeneous surface is shown as a dashed curve in Figure 5(b). The agreement with the true $f(V)$ is excellent at low energy, reproducing the broad maximum due to the heterogeneity.

The harmonic approximation to $f(V)$ can be further approximated by assuming that the behavior in the region of the potential energy minimum is the same for all \mathbf{R} , $D(\mathbf{R}) = D$ and $k(\mathbf{R}) = k$. This corresponds to a monolayer film on a flat surface, for which we choose as well depth the average value $D_{ave}(\mathbf{R})=180$ meV. In this case:

$$f_{flat}(V) = A \theta(V + D) \sqrt{\frac{2}{k(V + D)}}. \quad (3)$$

Here A is the computational surface area. Results of Equation 3 are shown in Figure 5(b) as the dotted curve. Notice that instead of a shoulder, $f_{flat}(V)$ exhibits a singularity at $V = -D_{ave}$; manifestly, the smooth surface approximation is not suitable for a QC.

At high energy, another approximation can be employed, which is related to the attractive part of the LJ potential. For a semi-infinite substrate, at positions far from the surface $V(z) = -C_3/z^3$, where $C_3 = (\pi/6) \sum_{i=1}^{\gamma} n_i C_6^{(i)}$ for a substrate composed of γ species of atoms, and $C_6^{(i)} = 4\epsilon_i \sigma_i^6$ is the coefficient of the attractive part in the usual LJ potential. Using this potential in Equation 1, we obtain:

$$f_{high}(V) = \frac{A}{3} \left(\frac{C_3}{|V|^4} \right)^{1/3} \quad (4)$$

Equation 4 is shown as dot-dashed curve in Figure 5(b). The approximation employed at high energy (dot-dash) does not match exactly the true $f(V)$ (full curve) since it assumes a semi-infinite substrate (which is not the case of the QC used in calculations) and since the volume considered in the numerical calculation extends to $z = \infty$ while in practice the numerical calculation stopped at $z_{max} = 10 \text{ \AA}$.

IV. ADSORPTION AT LOW COVERAGE

Adsorption at low coverages can be described in terms of a virial expansion [13, 20].

$$N_{excess} = k_H \beta P + C_{AAS} \beta^2 P^2 + \dots \quad (5)$$

The leading term of this expansion is all that is needed when the coverage is so low that interactions between adsorbate atoms can be neglected. In this regime, called the Henry's law regime, the coverage is proportional to the pressure (P) and the coefficient of proportionality is called the Henry's law constant:

$$k_H = \int d^3 \mathbf{r} [e^{-\beta V(\mathbf{r})} - 1]. \quad (6)$$

Here $\beta = 1/(k_B T)$ and $V(\mathbf{r})$ is the adsorbate-substrate interaction potential. At somewhat higher coverage, the interactions between adatoms become important and are taken into account through the second virial coefficient C_{AAS} :

$$C_{AAS} = \int d^3 \mathbf{r}_1 \int d^3 \mathbf{r}_2 e^{-\beta[V(\mathbf{r}_1) + V(\mathbf{r}_2)]} [e^{-\beta u(|\mathbf{r}_1 - \mathbf{r}_2|)} - 1] \quad (7)$$

where $u(|\mathbf{r}_1 - \mathbf{r}_2|)$ is the interaction between two adatoms. While the Henry's law coefficient involves a 3D integral which can be relatively easily calculated, the second virial coefficient is a 6D integral which is computationally expensive due to the large domain of integration.

Figure 6(a) presents an Arrhenius plot of the coverage (or excess number per unit area) as a function of $1/T$ for Xe and Ar in two regimes: very low coverage (Henry's law regime) and higher coverage (C_{AAS} included). At high T , the contribution of the second virial term is negligible, whereas at low T , mutual adatom interactions become important and the coverage is enhanced by the C_{AAS} term. However, when the second virial term greatly exceeds the first term, the virial expansion becomes divergent and its results cannot be trusted. Figure 6(b) presents a comparison of our calculated results with an experimental isobar. The agreement between calculation and experiment is rather good at low coverage (below $0.01 A^{-2}$) considering the simplicity of the model.

An interesting question arises in the heterogeneous environment of the QC potential: how does this heterogeneity affect the mutual adatoms' interactions? To investigate this, we compute the second virial coefficient in the 2D approximation [20]:

$$B_{2D} = -\frac{C_{AAS}}{2k_H^2} \quad (8)$$

On a substrate modelled as a flat 2D continuum, a monolayer film is perfectly mobile, so B_{2D} is not influenced by substrate but only by the adatoms' interaction $u(r)$:

$$B_{2D}^{flat} = -1/2 \int dr [e^{-\beta u(r)} - 1] \quad (9)$$

Figure 7 presents a comparison between B_{2D}/area for a flat substrate and for the QC. Note that the QC's corrugation enhances the effect of the adatoms' attraction since B_{2D} is larger in magnitude for a QC than for a flat substrate. We believe that this is another consequence of the aperiodicity and the semi-close packed structure of the QC. The increased attraction (also evident in the isosteric heat) occurs because the corrugated adsorption potential tends to bring particles closer together than a smooth surface. This effect is much stronger than in the case of a crystal, where the regular corrugated potential enhances the interactions' effect to a smaller extent [20].

The isosteric heat of adsorption can be computed from the equation of state:

$$Q_{st} = -\left(\frac{d \ln P}{d\beta}\right)_N \quad (10)$$

In the Henry's law regime, the isosteric heat reduces to:

$$Q_{st} = k_B T - \langle V \rangle \quad (11)$$

where $\langle V \rangle = (\int dr V e^{-\beta V}) / (\int dr e^{-\beta V})$ is the mean value of the adsorption potential. In the case of a flat substrate, assuming a harmonic adsorption potential, $\langle V \rangle = -D + k_B T/2$. Thus, the isosteric heat of a perfectly mobile monolayer on a flat surface increases monotonically with T as $Q_{st} = D + k_B T/2$. For a heterogeneous substrate, however, the dependence of Q_{st} on T must be determined numerically. Figure 8 presents the isosteric heat results for Xe and Ar in the Henry's law regime (coverage independent) and including the second virial coefficient correction (coverage dependent). Note that in both cases $Q_{st} \simeq D - k_B T/2$, meaning that $\langle V \rangle \simeq -D + 3k_B T/2$; this occurs because Xe atoms tend to be confined three-dimensionally on the QC (rather than 1D in the smooth surface mode). This finding is consistent with the very corrugated potential in Figure 3(b). A comparison between the Henry's law regime and second virial coefficient correction shows that the effect of interactions is to increase the isosteric heat. At T= 70 K, the calculated isosteric heat of Xe is 290 meV in the Henry's law regime and 305 meV when interactions are included. Both predictions are close to the value of 300 meV at 0.25 monolayer adsorption extracted from experimental isobars[12].

V. CONCLUSIONS

In conclusion, we have computed the adsorption potential of Xe and Ar adsorbates on Al-Ni-Co quasicrystalline substrate by adding gas-surface LJ interactions. Due to the substrate's aperiodicity and heterogeneity, the adsorption potential was found to be highly corrugated, with local minima ranging from -150 to -270 meV for Xe and -60 to -130 meV for Ar. The minimum energy surface of the adsorption potential exhibits the 5-fold symmetry of the QC's top layer, with the most repulsive regions located on top of the QC's atoms and the most attractive regions in the "holes" of the semi-close packed structure of the QC.

To understand the distribution of adsorption potential values, we have defined a volume density of states $f(V)$ and computed this quantity for QC, for a flat surface and for a harmonic approximation of the interaction potential. While $f_{flat}(V)$ exhibits a singularity when $V = -D$ (the well depth), $f_{QC}(V)$ has a broad maximum due to the QC's "heterogeneity". This shoulder is well reproduced by a local harmonic approximation of the adsorption potential in each point above the QC surface.

To model adsorption at low coverages, a virial expansion of the equation of state was employed, including first and second virial coefficient terms. Isobars obtained from the virial expansion agree well with experimental isobars of Xe on Al-Ni-Co QC. The isosteric heat of Xe was found to be 305 meV, close to experimental value of 300 meV at 0.25 monolayer. The dependence of the isosteric heat on T indicates that adatoms are 3D-confined in the attractive regions of the adsorption potential. This finding is consistent with the results of the second virial coefficient which suggest that the corrugation of the potential tends to bring adatoms together and enhance their mutual interactions. Future work will focus on a Monte Carlo study at arbitrarily high coverage and on a search for the adsorbate ground state structure.

VI. ACKNOWLEDGMENTS

We thank L.W. Bruch and G.D. Mahan for edifying comments and the National Science Foundation (Grants 02-08520 and 03-03916) for support of this research.

- [1] W. Steurer, T. Haibach, B. Zhang, S. Kek and R. Lck, *Acta Crystallographica B*, 49 (1993) 661.
- [2] A. Cervellino, T. Haibach and W. Steurer, *Acta Crystallographica B*, 58 (2002) 8.
- [3] H. Takakura, A. Yamamoto and A.-P. Tsai, *Acta Crystallographica*, A57 (2001) 576.
- [4] K. Saitoh, K. Tsuda, M. Tanaka, K. Kaneko and A.-P. Tsai, *Jpn. J Appl. Phys.*, 36 (1997) L1400.
- [5] P. J. Steinhardt, H. Jeong, K. Saitoh, M. Tanaka, E. Abe and A.-P. Tsai, *Nature*, 396 (1998) 55.
- [6] T. Haibach, A. Cervellino, M. A. Estermann and W. Steurer, *Philos. Mag. A*, 79 (1999) 933.
- [7] M. Mihalkovic, I. Al-Lehyani, E. Cockayne, C. L. Henley, N. Moghadam, J. A. Moriarty, Y. Wang and M. Widom, *Phys. Rev. B*, 65 (2002) 104205.
- [8] C. L. Henley, M. Mihalkovic and M. Widom, *J. Alloys Compd.*, 342 (2002) 221.
- [9] E. Cockayne and M. Widom, *Phys. Rev. Lett.* 81, 598 (1998).
- [10] E. Abe, K. Saitoh, H. Takakura, A.-P. Tsai, P. J. Steinhardt and H. C. Jeong, *Phys. Rev. Lett.* 84, 4609 (2000).
- [11] O. Zaharko, C. Meneghini, A. Cervellino and E. Fischer, *Eur. Phys. J. B* 19, 207 (2001).
- [12] N. Ferralis, K. Pussi, E.J. Cox, M. Gierer, J. Ledieu, I. R. Fisher, C. J. Jenks, M. Lindroos, R. McGrath, and R. D. Diehl, submitted to *Phys. Rev. Lett.* (2004).
- [13] L.W. Bruch, M.W. Cole and E. Zaremba, *Physical Adsorption: Forces and Phenomena*, Oxford University Press (1997)
- [14] P. Zeppenfeld. Noble Gases on Metals and Semiconductors, in *Physics of Covered Surfaces*, edited by H. P. Bonzel, Landolt- Boernstein, New Series, Group III, Vol 42, p. 67, Springer, Berlin (2001)
- [15] T. Fluckiger, Y. Weisskopf, M. Erbudak, R. Luscher, and A. R. Kortan, *NanoLetters* 3, 1717 (2003)

- [16] I. R. Fisher, M. J. Kramer, Z. Islam, A.R. Ross, A. Kracher, T. Wiener, M.J. Sailer, A.I. Goldman and P.C. Canfield, *Philos. Mag. B* 79, 425 (1999).
- [17] N.Ferralis, R.D.Diehl, K.Pussi, M.Lindroos, I.Fisher and C.J.Jenks, *Phys. Rev. B*, in press, (2004).
- [18] R. D. Diehl, J. Ledieu, N. Ferralis, A.W. Szmodis and R. McGrath, *Journal of Physics-Condensed Matter* 15, R63 (2003).
- [19] E.R. Moog, M.B. Webb, *Surf. Scie.* 148, 338 (1984)
- [20] W. A. Steele, “The Interaction of Gases with Solid Surfaces”, Pergamon Press, Oxford (1974)
- [21] J. L. F. Da Silva, C. Stampfl and M. Scheffler, *Phys. Rev. Lett.* 90, 066104 (2003)
- [22] R. McGrath, J. Ledieu, E. Cox, R.D. Diehl, *J. Phys. Condensed Matter* 14, R119-R144 (2002)
- [23] J. Ledieu, C.A. Muryn, G. Thornton. R.D. Diehl, T.A. Lograsso, D.W. Delaney and R. McGrath, *Surf. Sci.* 472, 89-96 (2001)
- [24] N. Jean, M. I. Trioni, G. P. Brivio, and V. Bortolani, *Phys. Rev. Lett.* 92 , 013201 (2004)
- [25] E. Conrad and M.B. Webb, *Surf. Sci.* 129, 37 (1983)
- [26] W.E. Packard and M.B. Webb, *Surf. Sci.* 195, 371 (1988)

VII. FIGURE CAPTIONS

1. One layer of a $45 \times 45 \text{ \AA}^2$ slab, representing one 5-fold plane of the d-AlNiCo quasicrystal surface, along the 10-fold axis. The atom colors correspond to sublayer groups differentiated according to the chemical identity and the local geometry (nearest neighbor distance): Red - Transition Metals (Ni or Co) 1, Black - Transition Metals 2, Green Al-1, Blue Al-2, Cyan Al-3, Yellow Al-4 [12].

2. LEED pattern from the 10-fold surface of the clean d-AlNiCo, acquired at 60 K. The incident energy was 55 eV.

3. Interaction potential energy between Xe (or Ar) and Al-Ni-Co QC: (a) Contour plot of the minimum energy surface. Different colors correspond to different isopotential curves: red = -175 meV, green = -200 meV, turquoise = -225 meV, blue = -250 meV; (b) Lateral variation of the minimum potential along two paths: $x = 1.6 \text{ \AA}$ (dashed curve) and $x = -1.6 \text{ \AA}$ (full curve).

4. The preferred adsorption regions at low coverage ($-270 \text{ meV} \leq V_{min}(r) \leq -220 \text{ meV}$).

5. Interaction potential energy between Xe and Al-Ni-Co QC: (a) Potential energy as a function of x for constant z above the QC, (b) The “volume density of states” of the QC (full curve), harmonic approximation limit at low energy (dashed), the high energy limit approximation (dot-dashed) and for a flat surface (dotted).

6. Coverage as a function of temperature (a) Arrhenius plot of Xe and Ar isobars at $P = 1.6 \times 10^{-7} \text{ mbar}$ in the Henry’s law regime (Ar-full, Xe-dot) and including the second virial term (Ar-dot-dash, Xe-dash), (b) Comparison of calculations with an experimental isobar of Xe at low coverage.

7. The second virial coefficient for a flat surface and the QC surface.

8. Isothermic heat of Xe and Ar on the QC in the Henry’s law regime: Xe (dashed), Ar (dotted), and including the second virial coefficient correction: Xe (full), Ar (dot-dashed).

This figure "fig1.jpg" is available in "jpg" format from:

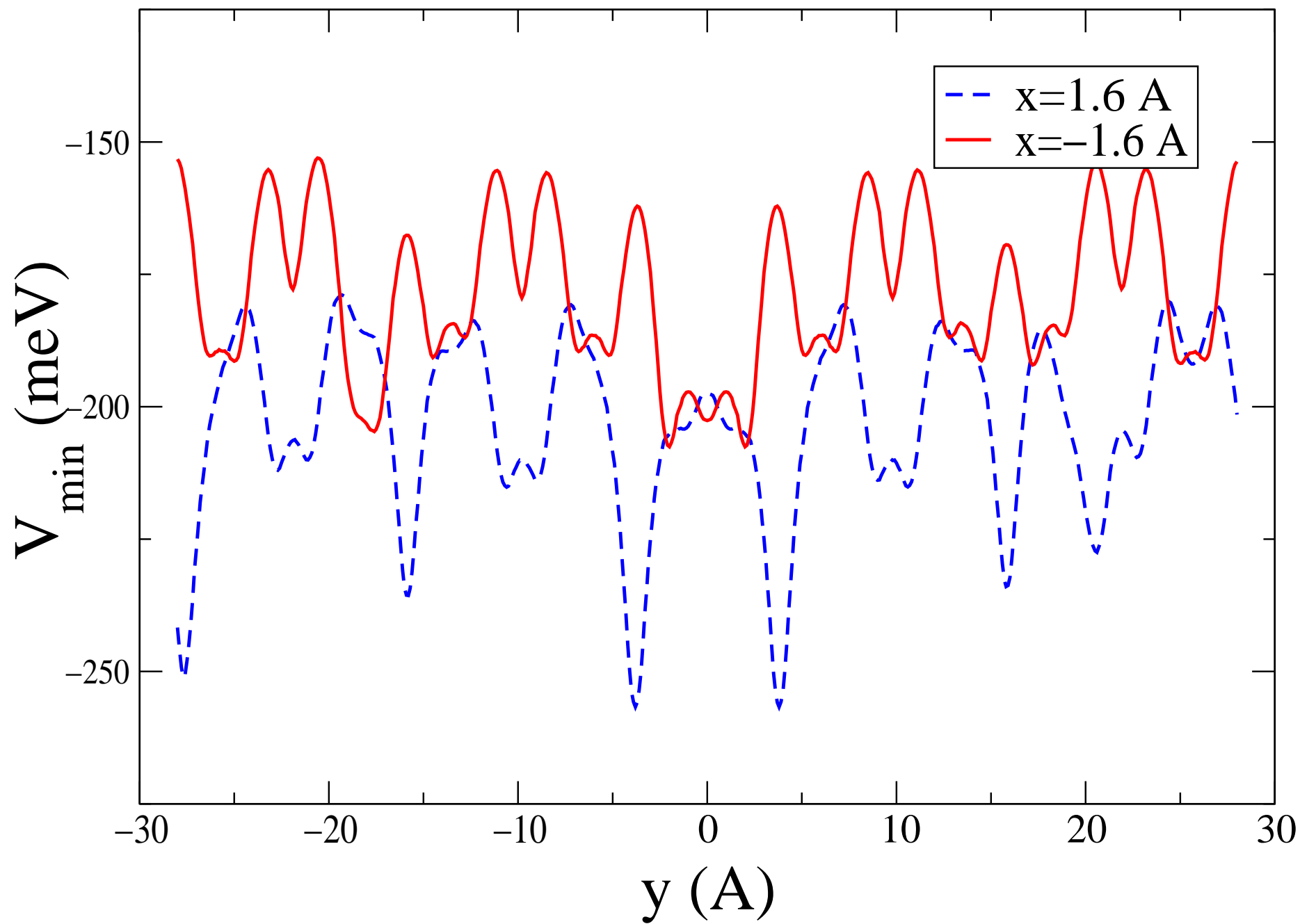
<http://arXiv.org/ps/cond-mat/0401467v1>

This figure "fig2.jpg" is available in "jpg" format from:

<http://arXiv.org/ps/cond-mat/0401467v1>

This figure "fig3a.jpg" is available in "jpg" format from:

<http://arXiv.org/ps/cond-mat/0401467v1>



This figure "fig4.jpg" is available in "jpg" format from:

<http://arXiv.org/ps/cond-mat/0401467v1>

